BIOCHEMISTRY
including biophysical chemistry & molecular biology

Article

pubs.acs.org/biochemistry

The Pathogenic Mutation T182A Converts the Prion Protein into a Molten Globule-like Conformation Whose Misfolding to Oligomers but Not to Fibrils Is Drastically Accelerated

Jogender Singh and Jayant B. Udgaonkar*

National Centre for Biological Sciences, Tata Institute of Fundamental Research, Bengaluru 560065, India

ABSTRACT: Delineation of the effects of pathogenic mutations linked with familial prion diseases on the structure and misfolding of prion protein (PrP) will be useful in understanding the molecular mechanism of PrP misfolding. Here, it has been shown that the pathogenic mutation T182A causes a drastic reduction in the apparent cooperativity and enthalpy of unfolding of the mouse prion protein (moPrP) under misfolding-prone conditions by converting the protein into a molten globule (MG)-like conformation. Hydrogen−deuterium exchange studies in conjunction with mass spectrometry indicate that the T182A mutation disrupts the core of the protein, thereby increasing overall structural dynamics. T182A moPrP is shown to misfold to oligomers very much faster than does wild-type (wt) moPrP but to misfold to fibrils at a rate similar to that of wt moPrP. This observation suggests that oligomers are unlikely to play a productive role in the direct pathway of aggregation from monomer to fibrils. The observation that fully folded T182A moPrP has a MG-like structure, and that it misfolds to oligomers much faster than does wt moPrP, suggests that a MG-like intermediate, whose structure resembles that of fully folded T182A moPrP, might be populated early on the pathway of misfolding of wt moPrP to oligomers.

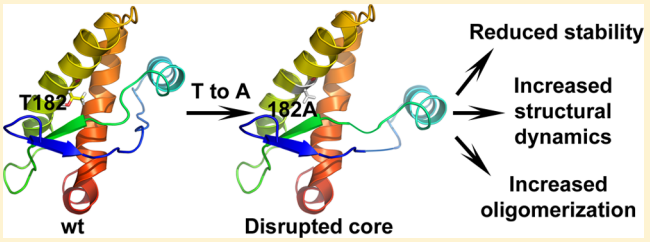

The prion protein (PrP) is a GPI-anchored protein expressed ubiquitously in the brain cells of mammals.[1] It is a glycoprotein with two N-linked glycosylation sites in its structured C-terminal domain.[2] The misfolding and aggregation of the cellular prion protein, PrP^{C}, into PrP^{Sc} (scrapie PrP), in the central nervous system, are linked with several fatal neurodegenerative disorders, which include familial Creutzfeldt−Jakob disease (fCJD), Gerstmann−Sträussler−Scheinker syndrome, and fatal familial insomnia.[3] While PrP^{C} is monomeric, highly soluble, proteinase K-sensitive, and α-rich, PrP^{Sc} is multimeric, insoluble, proteinase K-resistant, and β-rich.[3,4]

Misfolding of PrP can lead to oligomeric as well as fibrillar forms, including wormlike fibrils and straight fibrils.[5−7] Both the fibrillar[8−10] and oligomeric[11−16] forms have been shown to be toxic, *in vitro* and *in vivo*. It appears that oligomers and fibrils might have different roles in infectivity and toxicity in prion diseases.[17,18] Misfolded oligomers and fibrils formed *in vitro* resemble brain-derived PrP^{Sc}.[19−22] The structural cores of the oligomeric and fibrillar forms are similar,[19,21] but that of the straight fibrils is more extended and more stable than that of the other forms. Because these aggregated forms have undergone similar conformation conversion−dissolution of helix 1 (α1) and transformation of helices 2 (α2) and 3 (α3) into β-sheet,[21] it is conceivable that the oligomers are productive intermediates in the formation of straight fibrils. It is important to determine whether oligomers are on or off the pathway of straight fibril formation.

Misfolding to oligomers is favored at low pH and is linked to the protonation of a critical residue, which is characterized by a pK_a value of 4.7; hence, the extent of oligomer formation decreases with an increase in pH.[23,24] Although oligomers will be formed at physiological pH, they will not be populated to a detectable extent. On the other hand, the formation of straight fibrils is favored at physiological pH,[25] and amyloid fibril formation decreases with a decrease in pH.[5,7,25] It has therefore been difficult to determine what role, if any, oligomers play in the formation of straight fibrils. It appears that fibrils form directly from monomers at pH 7,[25] but this might merely be the consequence of an inability to detect oligomers at this pH. One way to establish the role of oligomers in fibril formation is to determine whether a mutation, especially a pathogenic mutation, that promotes the formation of oligomers also promotes the formation of straight fibrils.

A likely candidate for such a mutation is the T182A (mouse numbering, equivalent to human T183A; mouse numbering is used throughout this article) mutation at α2 in PrP (Figure 1a), which is known to cause early onset dementia.[26] Clinicopathological studies showed that this mutation leads to fCJD.[27] No amyloid plaques were, however, observed in the affected areas of the brain.[26,27] Interestingly, in the affected areas but not in the unaffected areas of the brain, no immunoreactivity was detected against monomeric PrP.[26] Hence, it is likely that the

Received: November 23, 2015
Revised: December 28, 2015
Published: December 29, 2015

DOI: 10.1021/acs.biochem.5b01266
Biochemistry 2016, 55, 459−469

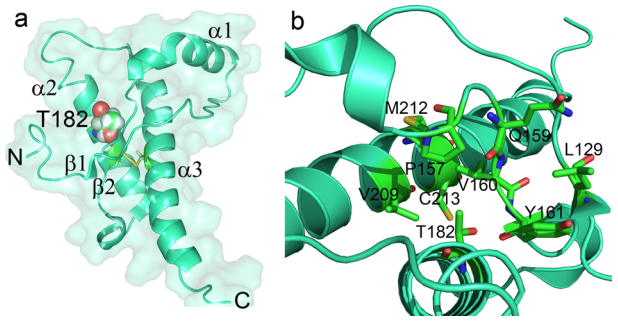

Figure 1. Structure of the C-terminal domain (residues 121−231) of the mouse prion protein highlighting residue T182. Residue stretch 23−120 is known to be unstructured in the full-length protein. (a) T182, which was mutated in this study, is labeled as spheres. The disulfide bond, which connects α2 and α3, is colored yellow. N and C represent the respective termini of the protein. (b) The side chain of T182 is 100% buried and appears to interact with L129, P157, Q159, V160, Y161, V209, M212, and C213. This figure was drawn using PyMOL and Protein Data Bank entry 1XYX.[74]

T182A mutation leads to the formation of misfolded oligomers rather than fibrils in the affected areas of the brain. Indeed, cell culture assays have shown the formation of misfolded oligomers by T182A human PrP.[28]

Many pathogenic mutations in PrP, which increase the likelihood of neurodegeneration,[3] appear to increase the likelihood of the misfolding of PrP^{C} into PrP^{Sc} (ref 29) by destabilizing the native protein.[22] Destabilization of the native state of a protein can lead to the population of partially unfolded forms of the protein,[30−34] some of which may be aggregation-prone.[33−35] One such partially unfolded form is the molten globule (MG) form, which has been implicated as a key early intermediate in the misfolding of many different proteins,[30,33,36−38] including the prion protein.[39−41] MG forms of a protein invariably possess a native-like fold with partial native-like secondary structure but appear to lack critical packing and tertiary interactions.[42] Identifying a pathogenic mutation of PrP that leads to the stabilization of a MG-like conformation at equilibrium would be of great utility for understanding how misfolding commences and for determining whether the mechanisms of misfolding to oligomers and to fibrils are similar.

Of the pathogenic mutations known to destabilize PrP, the T182A mutation is not only the most destabilizing but also the only pathogenic mutation that has been reported to affect folding cooperativity.[43] The mutation also appears to affect a significant conformational change in the protein: T182A bovine PrP, unlike wild-type (wt) PrP, can bind to PrP^{Sc}-specific antibodies.[44] Little is, however, known about how the mutation acts. Molecular dynamics studies give conflicting results: one study suggests that the mutation destabilizes α2 and α3 without affecting other regions,[45] while another study suggests that it causes the β-sheet to move away from the core of the protein.[46] Hence, it has become necessary to conduct an experimental characterization of the effects of the T182A mutation on the structure and dynamics of the protein, to understand the molecular basis of its effect on misfolding.

In this study, it is shown that the T182A mutation drastically reduces the cooperativity as well as enthalpy of unfolding of moPrP under misfolding-prone conditions, by converting the protein into a MG-like conformation. In this MG-like conformation, secondary structure appears to be modulated, and packing in the core of the protein is perturbed such that the structural dynamics in all segments of the protein have greatly increased. The T182A mutation causes the misfolding and oligomerization of moPrP to be greatly accelerated but has no effect on the kinetics of amyloid fibril formation.

MATERIALS AND METHODS

Reagents. All reagents used for experiments were of the highest purity grade available from Sigma, unless otherwise specified. Urea and guanidine hydrochloride (GdnHCl) were purchased from United States Biochemical Corp. and were of the highest purity grade.

Site-Directed Mutagenesis. The T182A mutation in the full-length mouse prion protein (moPrP) was generated using the QuikChange site-directed mutagenesis kit (Stratagene). Primers were obtained from Sigma. The mutation in the plasmid was confirmed by DNA sequencing.

Protein Expression and Purification. wt and T182A moPrP were expressed in *Escherichia coli* BL21(DE3) codon plus (Stratagene) cells upon transformation with a pET17b plasmid containing the full-length sequence (23−231) of the moPrP gene. The moPrP variants were purified as described previously.[6,23] Briefly, the cells were grown at 37 °C in rich medium containing 100 μg/mL ampicillin, and the protein was found to be expressed in inclusion bodies. Inclusion bodies were dissolved in a buffer containing 6 M GdnHCl, and purification and refolding were conducted on a Ni^{2+} Sepharose column (Amersham). The protein was further purified by reverse-phase chromatography using a Resource RPC column. The purity and mass of each moPrP variant preparation were confirmed by mass spectrometry (Waters Synapt G2 HD mass spectrometer). The protein was transferred to 10 mM sodium acetate buffer (pH 4) by using an Amicon ultrafiltration cell and stored at −80 °C. The protein concentration was determined from the absorbance at 280 nm, using an extinction coefficient of 62160 M^{-1} cm^{-1}.[6]

Removal of Any Aggregates Possibly Present in the Protein Preparations. The moPrP variant preparations were first incubated in 9 M urea at pH 4 and 25 °C for 30 min to denature any possible aggregates present. The proteins were then refolded in 10 mM sodium acetate (pH 4) using a Sephadex G-25 HiTrap desalting column in conjunction with an Akta Basic high-performance liquid chromatography system. Unfolding of a protein followed by refolding is one of the standard ways of removing any possible aggregates.[47,48]

Far-UV and Near-UV Circular Dichroism (CD) Measurements. Far-UV and near-UV CD spectra were recorded using a Jasco J-815 spectropolarimeter. Far-UV CD spectra were acquired using a protein concentration of 10 μM in a 1 mm cuvette, using a scan speed of 50 nm/min, a digital integration time of 2 s, and a bandwidth of 1 nm, and 15 spectra (scans) were averaged. Near-UV CD spectra were acquired using a protein concentration of 200 μM in a 2 mm cuvette, using a scan speed of 50 nm/min, a digital integration time of 2 s, and a bandwidth of 1 nm, and 200 spectra (scans) were averaged.

Oxidation Status of the Cysteine Residues of the moPrP Variants. The oxidation status of the cysteine residues of the moPrP variants was checked by treating the unfolded proteins with a 100-fold molar excess of 5,5′-dithiobis(2-nitrobenzoic acid) (DTNB) for 1 h. The details of the procedure are described elsewhere.[23]

DOI: 10.1021/acs.biochem.5b01266
Biochemistry 2016, 55, 459−469

Urea-Induced and Thermally Induced Equilibrium Unfolding Studies. Urea-induced and thermally induced equilibrium unfolding transitions were conducted at pH 4 in 10 mM sodium acetate buffer using 10 μM protein. The protein remained monomeric under these conditions.[49,50] These studies were conducted in the same way as described previously.[23] For the urea-induced unfolding, raw data were converted into fraction unfolded (f_U) values using eq 1:

$$f_U = \frac{Y_0 - (Y_F + m_F[D])}{Y_U + m_U[D] - (Y_F + m_F[D])} \quad (1)$$

where Y_0 is the CD value at a particular denaturant concentration, Y_F and Y_U represent the intercepts, and m_F and m_U represent the slopes of the native and unfolded protein baselines, respectively. f_U is related to the equilibrium constant, K_{app}, by the relationship $K_{app} = f_U/(1 - f_U)$, which is further related to the free energy as $\Delta G = -RT \ln K_{app}$. Hence, f_U is related to ΔG by a transformation of the Gibbs–Helmholtz equation as

$$f_U = \frac{\exp\left(-\frac{\Delta G + m_G[D]}{RT}\right)}{1 + \exp\left(-\frac{\Delta G + m_G[D]}{RT}\right)} \quad (2)$$

Thermally induced unfolding transitions were used to determine the apparent equilibrium constant, K_{app}, at any temperature using the following equation:

$$K_{app} = \frac{f_U}{1 - f_U} = \frac{Y_0 - (Y_F + m_F T)}{Y_U + m_U T - Y_0} \quad (3)$$

The changes in enthalpy (ΔH) associated with the unfolding transitions were obtained from van't Hoff plots of ln K_{app} versus $1/T$. The details of the analysis are described elsewhere.[50]

ANS Fluorescence Measurements. The moPrP variants, after treatment to remove any aggregates possibly present (see above), were mixed, at a concentration of 1 μM, with 8-anilinonaphthalene-1-sulfonic acid (ANS) at a final concentration of 10 μM at pH 4. The samples were incubated at room temperature for 30 min before fluorescence spectra were recorded. The fluorescence spectra were acquired from 400 to 600 nm, upon excitation at 365 nm.

Dynamic Light Scattering (DLS) Measurements. DLS measurements of the native proteins were taken at pH 4 and 25 °C using a DAWN 8+, eight-angle light scattering instrument (Wyatt Technology Corp., Santa Barbara, CA). The measurements were taken as described previously.[19] Measurements taken on protein samples that had been treated to remove any aggregates possibly present (see above) were found to be identical to measurements taken on protein samples that had not been so treated. For DLS measurements on oligomers, a DynaPro-99 unit (Protein Solutions Ltd.) was used. DLS measurements were taken at a protein concentration of 100 μM for oligomers. The measurements were taken as described previously.[6]

Oligomerization and Misfolding Studies at pH 4. Oligomerization and misfolding studies at pH 4 were essentially conducted in the same way as described previously.[23] Briefly, the protein in 10 mM sodium acetate buffer (pH 4) was diluted 2-fold with 2× oligomerization buffer [10 mM sodium acetate buffer and 300 mM NaCl (pH 4)], so that the protein was finally in 1× oligomerization buffer [10 mM sodium acetate buffer and 150 mM NaCl (pH 4)]. The samples were then incubated at 37 °C. The final protein concentration used for all the experiments was 100 μM. Oligomerization at different time points was then monitored by size exclusion chromatography (SEC). For studying the extent of oligomerization, a 100 μL aliquot of the incubated sample was taken out and injected into a Waters Protein Pak 300-SW column using an Akta (GE) chromatography system kept at 25 °C. The column was equilibrated with 4 column volumes of 1× oligomerization buffer at pH 4 (10 mM sodium acetate buffer and 150 mM NaCl), after several samples of oligomer had first been run through the column. In all subsequent SEC experiments, the amounts of oligomer and monomer that eluted out were found to account for all the protein that had been injected into the column. The areas of the monomer and oligomer peaks were calculated by fitting the SEC profiles to multiple peaks, using Origin Pro 8. The fraction monomer left was calculated from the area under the monomer peak in SEC divided by the total area under all peaks. The fraction oligomer formed was then calculated by subtracting fraction monomer from 1. Concurrently, the samples were diluted to 10 μM in 1× oligomerization buffer, and far-UV CD spectra were acquired.

For studying the misfolding rates of T182A moPrP, oligomerization experiments under the same conditions as described above were conducted using a 0.5 mm water-jacketed quartz cuvette at 37 °C, and the kinetics were monitored by CD. All the solutions were incubated at 37 °C before the reaction was started. The reaction was started by mixing either 200 or 100 μM moPrP in equal amounts with 2× oligomerization buffer and then immediately incubating the sample in the cuvette that was maintained at 37 °C using a water bath. The final protein concentration was either 100 or 50 μM. The time from the mixing of the protein with 2× oligomerization buffer to the first reading was ~40 s. Because the change in the CD signal at 228 nm, as native monomer converts to misfolded oligomers, is substantial, and because the kinetics at 228 nm is similar to that at 216 nm,[22] the time course of the change in the CD signal was conducted at 228 nm, where the signal-to-noise ratio is better.

Measurements taken on protein samples that had been treated to remove any aggregates possibly present (see above) were found to be identical to measurements taken on protein samples that had not been so treated.

Fibril Formation at pH 7. Fibrillization at pH 7 was conducted in 96-well plates in a Fluoroskan Ascent plate reader. To start fibrillization, the protein in 10 mM sodium acetate buffer (pH 4) was diluted 2-fold with 2× aggregation buffer [100 mM Tris-HCl and 4 M GdnHCl (pH 7.45)], so that the protein was finally in 1× aggregation buffer [50 mM Tris-HCl and 2 M GdnHCl (pH 7)]. The final protein concentration used for all the experiments was 20 μM; 50 μM ThT was added to the reaction samples. The protein in 1× aggregation buffer was then transferred to different wells of a 96-well plate in volumes of 200 μL, incubated at 37 °C, and shaken at 480 rpm using the Fluoroskan Ascent plate reader. The ThT fluorescence was measured at 475 nm upon excitation at 445 nm. ThT readings were acquired every 10 min.

Measurements taken on protein samples that had been treated to remove any aggregates possibly present (see above) were found to be identical to measurements taken on protein samples that had not been so treated.

Atomic Force Microscopy (AFM). Samples for AFM were prepared as described previously.[23] AFM images were obtained

DOI: 10.1021/acs.biochem.5b01266
Biochemistry 2016, 55, 459–469

using a Bruker FastScan AFM instrument operating in noncontact mode.

HDX-MS Measurements. The peptide map of the moPrP variants was generated as described previously.[19] HDX-MS measurements were taken as described previously.[23] For calculation of the protection factors (P_f), the observed HDX rate curve (k_{obs}) for a peptide fragment, which was obtained by fitting to a monoexponential or biexponential curve depending upon the goodness of fit, was compared to a reference (intrinsic) curve (k_{int}) expected for the peptide in a random coil state.[51,52] The HDX protection factor for a peptide was determined as $P_f = k_{int}/k_{obs}$. P_f for a peptide was used to calculate the local stability ΔG of the segment corresponding to the peptide ($\Delta G = RT \ln P_f$).

RESULTS AND DISCUSSION

The T182A Mutation Induces Changes in the Secondary and Tertiary Structure of wt moPrP. Recombinant wt full-length mouse PrP (moPrP) was mutated to T182A moPrP by site-directed mutagenesis. T182A moPrP showed a far-UV circular dichroism (CD) spectrum typical for a helical protein (Figure 2a), but the spectrum showed a

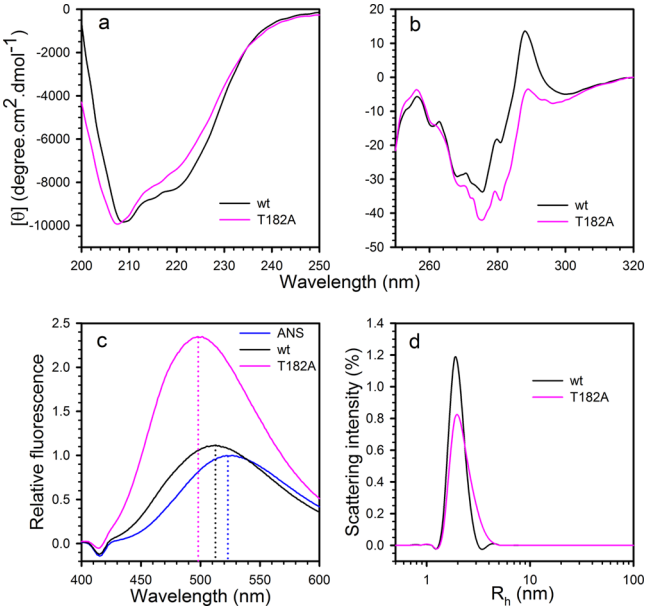

Figure 2. Biophysical characterization of native monomeric wt and T182A moPrP at pH 4. (a) Far-UV CD and (b) near-UV CD spectra of wt and T182A moPrP. The spectra were acquired in 10 mM sodium acetate buffer at pH 4 and 25 °C. (c) Relative fluorescence of 10 μM ANS in the absence and presence of 1 μM wt and T182A moPrP at pH 4 and 25 °C. The signals are normalized with respect to that of 10 μM ANS. ANS shows emission maxima in the absence and presence of wt and T182A moPrP of 523, 512, and 499 nm, respectively, as shown by the respective vertical lines. (d) Hydrodynamic radii (R_h) of wt and T182A moPrP, as determined from dynamic light scattering measurements at pH 4, 25 °C, and 100 μM protein.

perturbation in its shape as well as a reduction in mean residual ellipticity at 222 nm, compared to that of wt moPrP. These changes had not been seen for other destabilized mutant variants of moPrP.[22] It therefore appears that T182A moPrP has less secondary structure than wt moPrP. Moreover, T182A moPrP showed a near-UV CD spectrum significantly different from that of wt moPrP (Figure 2b), suggesting that the mutation has perturbed the tertiary structure, as well. Interestingly, the near-UV CD spectrum of T182A moPrP at pH 4, where wt moPrP is fully native, is very similar to that of a MG form of wt PrP formed at pH 2.[40]

T182A moPrP Exists as a Molten Globule-like Form. The observations that the T182A mutation caused a reduction in the level of secondary structure and perturbed the tertiary structure of the protein under native conditions suggested the possibility that T182A moPrP might exist as a MG-like form under native conditions. MG forms of proteins are swollen forms of the native state, usually with reduced secondary structure and with perturbed tertiary structure, but with a very similar topology.[42] Residues are less tightly packed than in the native state; consequently, the MG form possesses hydrated hydrophobic surfaces to which hydrophobic dyes such as 8-anilinonaphthalene-1-sulfonic acid (ANS) can bind.[53] To confirm whether T182A moPrP exists as a MG-like form, ANS binding was studied. When ANS binds to hydrophobic patches, its fluorescence emission undergoes a blue shift as well as an increase in intensity. An ~2.5-fold increase in ANS fluorescence intensity, as well as an ~25 nm blue shift in the wavelength of maximum emission (Figure 2c), was observed in the presence of T182A moPrP. On the other hand, the presence of wt moPrP did not increase the ANS fluorescence significantly, although an ~10 nm blue shift in the wavelength of maximum emission was observed. The ANS binding results remained unchanged for the two proteins after they were passed through a 50 or 100 kDa molecular weight cutoff filter (data not shown), confirming that ANS was binding to monomeric protein.

In a detailed thermodynamics study[50] of the unfolding of wt moPrP at pH 4, the native state heat capacity was shown to be significantly larger than those of proteins of comparable size, indicating that the native state of wt moPrP undergoes substantial enthalpic and structural fluctuations that expose otherwise hydrophobic residues. Not surprisingly, the protection factors for backbone amide hydrogen exchange in wt moPrP at pH 4 are substantially lower than those of other globular proteins.[54,55] The lower protection factors of wt moPrP suggest looser packing and a hydrophobic core that may be partially accessible to water and, hence, to ANS. This is likely to be the reason why a small blue shift in ANS fluorescence was observed even in the presence of wt moPrP (Figure 2c).

It should be noted that the structural changes in the protein caused by the T182A mutation were not caused by protein oligomerization: both wt and T182A moPrP were shown by dynamic light scattering (DLS) measurements to exist as monomers under the conditions studied (Figure 2d). There was no evidence of any oligomer present in the absence of added 150 mM NaCl, even at a protein concentration of 100 μM, which was the highest protein concentration used for any measurement in this study (see Materials and Methods). Moreover, the structural changes were not caused by covalent modification of the proteins. The masses of both proteins, as determined by mass spectrometry, were those expected for the proteins without any chemical modifications (Figure 3).

The Thermodynamic Stability and Cooperativity of the Unfolding Transition of T182A moPrP Are Drastically Reduced. Denaturant-induced unfolding studies showed that the thermodynamic stability of T182A moPrP was substantially lower than that of wt moPrP at pH 4 (Figure 4a and Table 1) T182A moPrP is also known to have a drastically

DOI: 10.1021/acs.biochem.5b01266
Biochemistry 2016, 55, 459−469

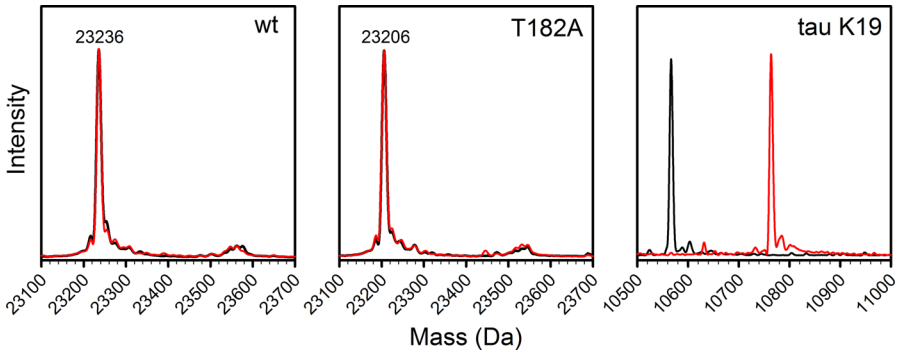

Figure 3. Oxidation status of the cysteine residues in the moPrP variants. Mass spectra of the moPrP variants before (black) and after (red) DTNB treatment in 6 M guanidine hydrochloride (GdnHCl) (see Materials and Methods). The masses of the proteins were the same as those of the untreated proteins, indicating that the disulfide bond is intact in all the protein molecules. Mass spectra of tau K19 protein before (black) and after (red) DTNB treatment in 6 M GdnHCl are also shown as a control: a mass difference of +198 Da was observed upon labeling as expected.

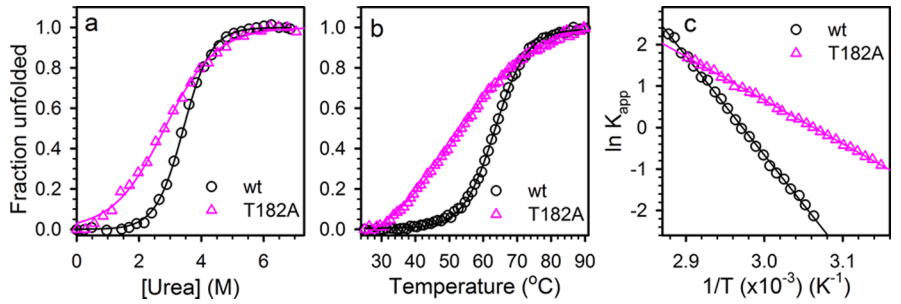

Figure 4. Thermodynamic stabilities of wt and T182A moPrP at pH 4. (a) Urea-induced equilibrium unfolding transitions at pH 4 and 25 °C as monitored by far-UV CD at 222 nm. (b) Thermal unfolding of wt and T182A moPrP at pH 4 as monitored by far-UV CD at 222 nm. The signals were normalized to determine the fraction unfolded. (c) Linear least-squares fits through van't Hoff plots (ln K_{app} vs $1/T$) obtained from the thermal denaturation curves.

Table 1. Thermodynamic Parameters Obtained from Urea-Induced and Thermally Induced Equilibrium Unfolding Studies of the moPrP Variants at pH 4[a]

protein	ΔG (kcal mol^{-1})	m (kcal mol^{-1} M^{-1})	C_m (M)	T_m (°C)	ΔH (kcal mol^{-1})
wt	4.5 ± 0.4	1.29 ± 0.04	3.49 ± 0.08	64.1 ± 0.9	47 ± 1.1
T182A	1.9 ± 0.2	0.68 ± 0.05	2.79 ± 0.07	52.7 ± 1.3	21 ± 0.2

[a]Errors represent the standard deviations determined from three independent experiments.

reduced thermodynamic stability at pH 7.[43] Interestingly, the m-value, which is indicative of the change in surface area during unfolding, was also dramatically reduced for T182A moPrP compared to that of wt moPrP (Table 1). Thermally induced unfolding studies also showed a significant reduction in stability: the temperature of unfolding (T_m) of T182A moPrP is drastically lower than that of wt moPrP (Figure 4b and Table 1). Moreover, the thermally induced unfolding transition of T182A moPrP was very broad compared to that of wt moPrP. The change in enthalpy associated with the unfolding transition was obtained from van't Hoff plots of ln K_{app} versus $1/T$ (Figure 4c) and was found to be drastically reduced for T182A moPrP compared to that of wt moPrP (Table 1). Clearly, the T182A mutation has reduced the cooperativity of the unfolding transition. Broad unfolding transitions are characteristic of MGs,[42,56] and these results are consistent with T182A moPrP adopting a MG-like conformation.

Because it is known that the disulfide bond in PrP is important for its conformational stability,[57] it was important to establish that the observed difference in stability between wt and T182A moPrP is not caused by the disulfide bond having become reduced for the proteins during measurement. This was done by checking whether the denaturant-unfolded proteins were amenable to labeling by the thiol reagent DTNB; they were found not to be so (Figure 3). Hence, the decrease in the stability of T182A moPrP was not because of a difference in its oxidation status.

T182A moPrP Shows Increased Structural Dynamics in Most of the Secondary Structure Regions. The observation that T182A moPrP showed a drastic reduction in the thermodynamic stability and cooperativity of its unfolding transition made it important to determine the extent to which the mutation also affects the structural dynamics of the protein. To this end, hydrogen−deuterium exchange studies coupled with mass spectrometry (HDX-MS) were conducted to obtain sequence-specific structural information. In HDX-MS studies, the amide hydrogen sites that are protected against HDX can be localized to specific segments of the protein sequence by proteolytic fragmentation at low pH, after the HDX reaction is complete. A peptide map generated previously[19] was used for the study presented here. For HDX-MS studies, the native monomeric protein in H_2O buffer was diluted 20 times in D_2O buffer at pH 4. The protein was then allowed to become labeled in D_2O at 25 °C. At different times of labeling, an aliquot was

DOI: 10.1021/acs.biochem.5b01266
Biochemistry 2016, 55, 459−469

withdrawn, mixed with ice-cold quench buffer (pH 2.5), and then immediately injected into the HDX module for online pepsin digestion at low pH. The peptic fragments were then separated and infused into the MS instrument to determine their masses. In this study, misfolding leading to oligomer formation was studied at pH 4 because PrP is much more prone to misfolding and oligomer formation at this pH than at higher pH,[23,54] for reasons stated elsewhere.[23] Hence, HDX into the native protein was conducted at the same pH. pH 4 is also close to the pH at which intrinsic HDX rates are at their minimum. This allows HDX to be observed at amide hydrogen sites spread over all the secondary structural elements of the protein.

Deuterium incorporation profiles for different sequence segments fit to a monoexponential or biexponential equation (Figure 5). Biexponential kinetics of exchange for a sequence

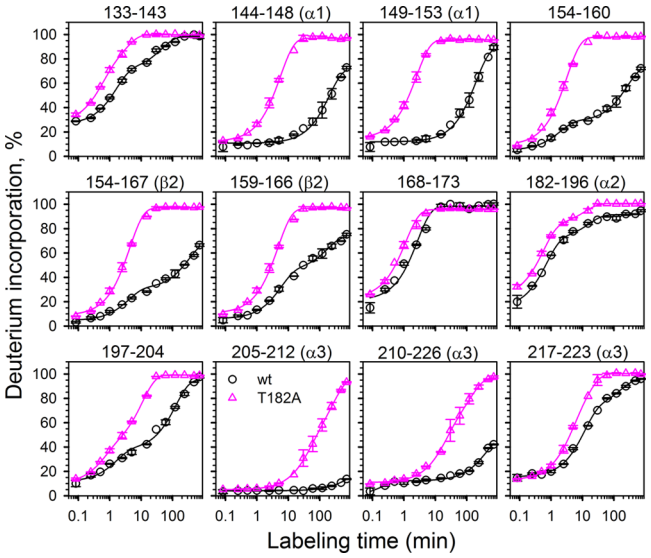

Figure 5. Time course of HDX into different secondary structural regions of monomeric T182A and wt moPrP at pH 4. Percent deuterium incorporation profiles at pH 4 and 25 °C of selected sequence segments are shown. Error bars represent the standard deviations determined from three independent experiments. The solid lines through the data represent the fits to either monoexponential or biexponential equations.

segment likely arose from the presence of different secondary structural units in the segment, which differed in the extents to which they are protected against HDX. It is unlikely that the biexponential kinetics of exchange for a sequence segment arose because partially folded monomeric protein was present along with fully folded native monomer. The coexistence of partially folded and fully folded monomer would have led to a bimodal mass distribution for the sequence segment that was structured in one conformation and unstructured in the other, but all the sequence segments for both wt and T182A moPrP were found to show unimodal mass distributions (data not shown). Most of the secondary structure regions showed increased deuterium incorporation rates in T182A moPrP compared to the rates observed for wt moPrP (Figure 5). This indicated that all these secondary structure regions had increased structural dynamics, as manifested by lower protection factors against HDX, compared to those seen for wt moPrP (Table 2 and Figure 6). Some sequence segments that displayed biexponential kinetics of HDX in wt moPrP displayed monoexponential kinetics of HDX in T182A moPrP. This was most likely because the slower of the two rates for such a segment had increased in T182A moPrP, so that two rates for the segment could no longer be distinguished. The rates of deuterium incorporation were, however, seen to increase differently in different secondary structure regions. The sequence segments covering α1, the loop between α1 and β-strand 2 (β2), and α3 regions showed the most pronounced increases in deuterium incorporation rates compared to those of other regions (Figures 5 and 6). Residue 182 is located in α2, and hence, the T182A mutation was also expected to increase the rate of incorporation of deuterium into sequence segment 182−196, which spans the sequence covering the C-terminal region of α2. The rate of incorporation of deuterium into this sequence segment of wt moPrP was, however, already quite fast: it was only slightly slower than the intrinsic rate of exchange, with a very low protection factor (Table 2). While the mutation did have a local structural effect on sequence segment 182−196 (Figure 5 and Table 2), the effect appeared to be small (Figure 6) only because the protection was so low in the wt protein itself.

T182A moPrP Shows a Drastic Increase in Misfolding Rate to Oligomers at pH 4. MG forms of many proteins are known to be aggregation-competent.[33,37,38] MG forms can lead to the formation of oligomeric as well as fibrillar structures.[37,38] Hence, it was important to determine how the MG-like form of moPrP formed by the mutation T182A affected its misfolding and oligomerization. The addition of salt is known to induce misfolded oligomer formation in PrP under denaturing[49,58] and nondenaturing conditions.[23] Moreover, salt is known to modulate misfolding pathways of moPrP.[59] Hence, to determine the effect of the drastic changes in the structural dynamics of T182A moPrP on its oligomerization and misfolding, 100 μM T182A moPrP was incubated at 37 °C in the presence of 150 mM NaCl (pH 4). Under these conditions, wt moPrP is known to take 24 h to oligomerize to completion,[23] as observed by size exclusion chromatography (SEC) (Figure 7). In contrast to wt moPrP, T182A moPrP oligomerized very rapidly (Figures 7 and 8a). After being incubated for 5 min, it showed complete oligomerization (Figure 7).

The oligomers formed by both proteins were misfolded and β-sheet-rich as monitored by CD (Figure 8b). wt moPrP oligomers appeared to have a hydrodynamic radius slightly larger than that of T182A moPrP oligomers, as observed by DLS measurements (Figure 9a). Atomic force microscopy (AFM) images showed that the oligomers formed by both wt and T182A moPrP were spherical in shape, and that wt moPrP oligomers had heights (diameters) greater than that of T182A moPrP oligomers (Figure 9b,c). Oligomers of different heights were observed for both wt and T182A moPrP. Both large and small oligomers were observed to have been formed by T182A moPrP (Figure 7), as they are for wt moPrP.[23]

Because the oligomerization of T182A moPrP was too rapid to measure by SEC, its misfolding was monitored by CD. wt moPrP is known to take ~24 h to completely misfold, at a rate similar to the rate of oligomerization (Figure 8b). On the other hand, T182A moPrP misfolded very rapidly: it misfolded to ~90% within 40 s of mixing of the protein with oligomerization buffer (Figure 8c). Misfolding occurred too rapidly for its rate to be accurately determined. Even at 50 μM protein, T182A moPrP showed a very rapid rate of misfolding to oligomers (Figure 8c). Hence, the thermodynamic destabilization and

DOI: 10.1021/acs.biochem.5b01266
Biochemistry 2016, 55, 459−469

Table 2. Protection Factors (P_f) for Different Sequence Segments of wt and T182A moPrP[a]

sequence segment	k_{int} (min^{-1}) at pD 4	k_{obs} (min^{-1}) for wt	k_{obs} (min^{-1}) for T182A	P_f (wt)	P_f (T182A)
133–143	0.55	0.63 ± 0.12 (61%)	2 ± 0.7 (53%)	1	0.3
		(2.26 ± 0.18) × 10^{-2} (39%)	0.34 ± 0.05 (47%)	24	1.6
144–148	1.36	(4.89 ± 0.58) × 10^{-3}	0.18 ± 0.01	278	7.5
149–153	1.05	(5.10 ± 0.52) × 10^{-3}	0.39 ± 0.04	206	2.7
154–160	0.33	0.52 ± 0.03 (34%)	0.31 ± 0.02	0.6	1
		(3.85 ± 0.11) × 10^{-3} (66%)		86	
154–167	0.25	0.26 ± 0.02 (40%)	0.23 ± 0.01	1	1
		(2.97 ± 0.13) × 10^{-3} (60%)		84	
159–166	0.13	0.17 ± 0.01 (57%)	0.21 ± 0.01	1	0.6
		(5.68 ± 0.22) × 10^{-3} (43%)		23	
168–173	0.98	0.37 ± 0.08	0.88 ± 0.12	2.6	1.1
182–196	0.53	1.41 ± 0.11 (73%)	1.80 ± 0.19 (76%)	0.4	0.3
		(6.17 ± 0.57) × 10^{-2} (27%)	(8.66 ± 1) × 10^{-2} (24%)	9	6
197–204	0.52	0.62 ± 0.08 (31%)	1.58 ± 0.2 (30%)	1	0.3
		(7.90 ± 0.42) × 10^{-3} (69%)	(9.31 ± 0.42) × 10^{-2} (70%)	66	5.6
205–212	0.30	ND[b]	(8.67 ± 2.34) × 10^{-3}	ND[b]	35
210–226	0.41	(2.45 ± 0.14) × 10^{-3}	(2.00 ± 0.58) × 10^{-2}	167	21
217–223	0.61	(8.88 ± 0.77) × 10^{-2} (68%)	(12 ± 0.15) × 10^{-2}	7	5
		(6.25 ± 0.28) × 10^{-3} (32%)		98	

[a]A single k_{obs} for a sequence segment was obtained from a fit to a monoexponential equation, while two k_{obs} values for a sequence segment were obtained from a fit to a biexponential equation. The percent amplitudes for two rates were calculated as $[a_i/(a_1 + a_2)] \times 100$ (where a_i is either a_1 or a_2). The values of the protection factors shown for some of the sequence segments of wt moPrP are likely to have been underestimated because deuterium incorporation was not measured at sufficiently long times. Errors represent the standard deviations determined from three independent experiments. [b]Not determined.

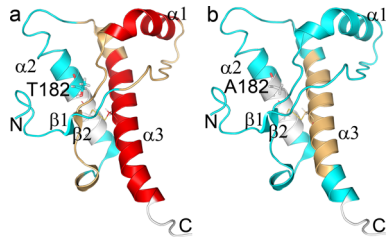

Figure 6. Protection of wt and T182A moPrP against HDX at pH 4. Protection factors mapped onto the secondary structure of (a) wt and (b) T182A moPrP. Cyan, light orange, and red colors represent protection factors of 1–10, 10–100, and >100, respectively. White color represents regions of the protein that are missing in the peptide map. The structures were drawn using PyMOL and Protein Data Bank entry 1XYX.[74] See Table 2 for protection factors for different regions.

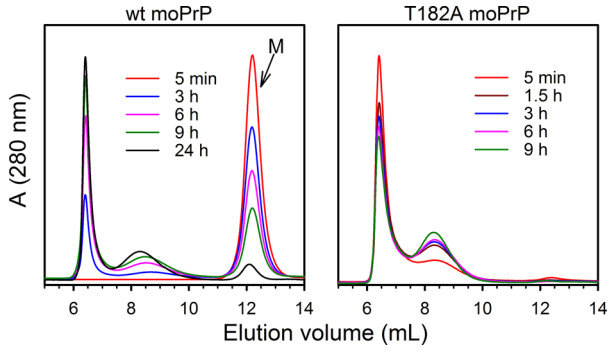

Figure 7. Time course of oligomerization of the moPrP variants in 150 mM NaCl at 37 °C, pH 4, and 100 μM protein, as monitored by size exclusion chromatography. M represents the monomer peak.

increased structural dynamics of T182A moPrP appeared to have led to a drastic increase in its rate of misfolding to oligomers. It should be noted that a previous study had shown that other destabilizing pathogenic mutations also lead to an acceleration of misfolding,[22] but none of those mutant variants possessed any of the MG-like features shown by T182A moPrP.

The T182A Mutation Does Not Affect Amyloid Fibril Formation by moPrP. To determine if the T182A mutation affected the formation of straight amyloid fibrils by moPrP, fibrillization experiments were conducted. In previous studies of the fibrillization of different PrPs at pH 7, fibrillation was invariably conducted under denaturing conditions, in the presence of 2 M guanidine hydrochloride (GdnHCl).[23,60−62] In the study presented here, too, fibrillization experiments at pH 7 were conducted in the presence of 2 M GdnHCl. Under these conditions, moPrP has been shown, by AFM imaging, to form straight amyloid fibrils.[23] Surprisingly, the T182A mutation did not show any effect on fibril formation. The kinetics of fibril formation were very similar for T182A and wt moPrP (Figure 10a). Both proteins formed amyloid fibrils that had heights of 6–8 nm as monitored by AFM (Figure 10b,c). The amyloid fibrils formed by both proteins appeared to be similar in morphology. Thus, the reduction in the thermodynamic stability and increased structural dynamics of moPrP, caused by the T182A mutation, did not affect its ability to form straight amyloid fibrils. It is important to note, however, that the addition of 2 M GdnHCl to induce fibril formation might have minimized conformational differences between wt and T182A moPrP and thereby subtly altered the aggregation kinetics. In future studies, it would be interesting to determine if the fibrillization kinetics of the two proteins differ from each other at different concentrations of GdnHCl.

The current observation indicated that the pathways and the molecular mechanisms of formation of misfolded amyloid oligomers and of straight amyloid fibrils by PrP are likely to be different. As the formation of misfolded oligomers and the formation of amyloid fibrils are favored at different pH values (see above), it is likely that electrostatic interactions play an

DOI: 10.1021/acs.biochem.5b01266
Biochemistry 2016, 55, 459−469

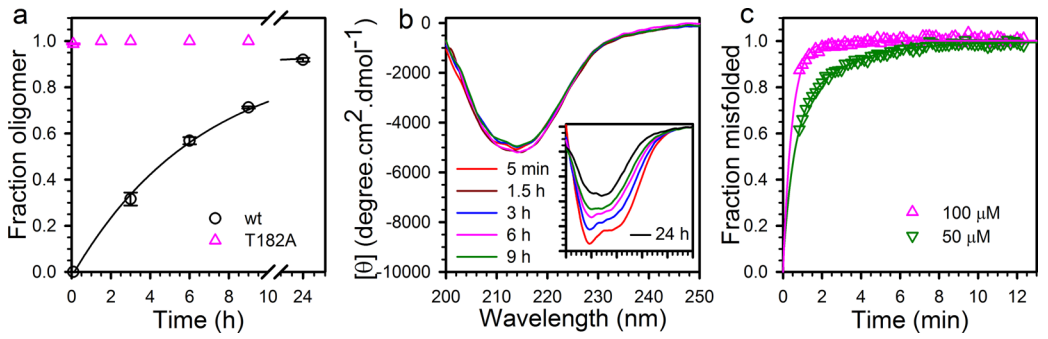

Figure 8. Misfolded oligomer formation by the moPrP variants. (a) Fraction oligomer formed at different times of aggregation of the moPrP variants. The reaction was conducted in the presence of 150 mM NaCl, at 37 °C, pH 4, and at 100 μM protein. The oligomer formed was quantified by SEC. (b) Time course of conformational conversion of T182A moPrP in 150 mM NaCl, at 37 °C, pH 4, and 100 μM protein, as monitored by far-UV CD spectra. The inset shows the time course of conformational conversion of wt moPrP under the same conditions. The *x*- and *y*-axis scales in the inset are the same as in the main figure. (c) Fraction misfolded protein at different times of reaction for T182A moPrP at 100 and 50 μM protein. The misfolded fraction was calculated by normalizing the MRE at 228 nm with respect to the wt moPrP signal at 72 h of aggregation under the same conditions as in panel b.

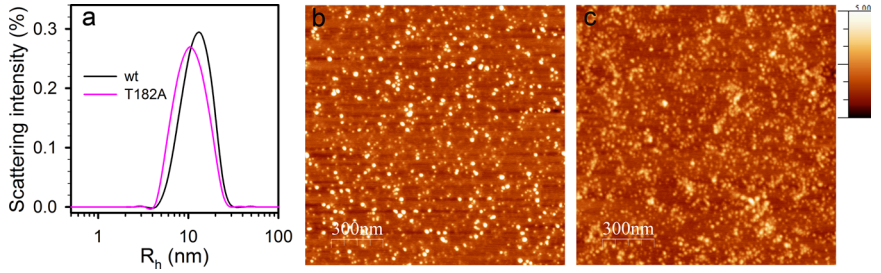

Figure 9. Characterization of the size and morphology of oligomers of the moPrP variants formed at pH 4. (a) Distribution of the size of oligomers formed by wt and T182A moPrP as probed by dynamic light scattering. AFM images of (b) wt and (c) T182A moPrP oligomers. The measurements were taken after aggregation of T182A and wt moPrP for 30 min and 24 h, respectively. The *Z*-scale for both the images is 5 nm.

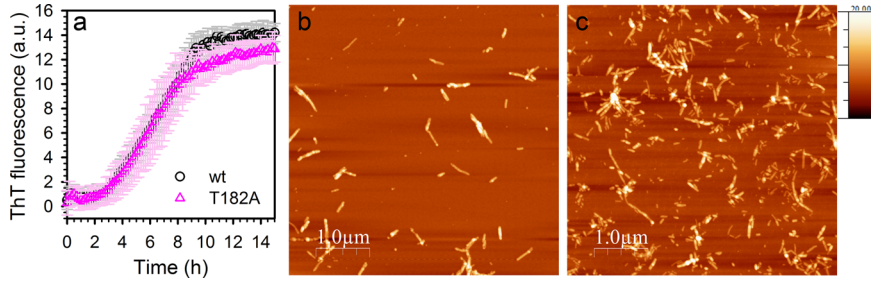

Figure 10. Fibrillization of wt and T182A moPrP at pH 7. (a) Kinetics of fibril formation by the moPrP variants probed by ThT fluorescence measurements at pH 7. Error bars represent the standard deviations from three independent experiments. AFM images of the aggregates formed by (b) wt and (c) T182A moPrP. AFM images were acquired after aggregation of both proteins for 15 h. The *Z*-scale for both the images is 20 nm.

important role in determining the pathway of aggregation. For instance, the deprotonation of some critical residues might be linked to the conformational change accompanying the formation of amyloid fibrils at high pH values. Conversely, the protonation of some critical residues might be linked to misfolded oligomer formation at low pH values. The details of such mechanisms remain, however, to be determined.[21]

The T182A Mutation Appears To Disrupt the Structural Core of moPrP. Although T182A moPrP showed increased structural dynamics in almost all the secondary structure regions (Figure 5), the increase in structural dynamics was the most pronounced in α1 and the loop between α1 and β2 and α3 regions. The side chain of T182 is completely buried in the hydrophobic core of the protein where it interacts with the side chains of L129, P157, Q159, V160, Y161, V209, M212, and C213 (Figure 1b), which are present in the β-sheet, α3, and the loop between α1 and β2. The T182A mutation would lead to the loss of these packing interactions and, hence, to the disruption of the core of the protein. The disruption of the core of the protein would lead to an increased rate of deuterium incorporation in T182A moPrP (Figure 5). Mutations that disrupt the core of a protein are known to destabilize the protein.[63,64]

The enthalpy of unfolding of T182A moPrP was found to be less than half of that of wt moPrP (Table 1). Such a reduction in the enthalpy of unfolding upon mutation has been shown to be linked to a reduction in the level of packing interactions, for various proteins.[65] This is not surprising as hydrophobic packing interactions are known to be very crucial for the stability of a protein.[63,64] The reduction in the level of packing interactions in T182A moPrP compared to that in wt moPrP is

DOI: 10.1021/acs.biochem.5b01266
Biochemistry 2016, 55, 459−469

likely to be the reason why HX occurs faster in all regions of the mutant protein.

The disruption of the core of the protein led to drastic reductions in the stabilities of the α1 and α3 regions in T182A moPrP. These structural changes led to a very drastic increase in the rate of misfolded oligomer formation (Figure 8). Interestingly, a mutation in α3, which thermodynamically stabilizes the protein, has been shown to reduce the level of human PrP misfolding.[66] Moreover, thermodynamic stabilization of α2 of moPrP is known to prevent its misfolding.[23] Because the α2−α3 region is known to undergo major conformational changes during misfolding,[19,21,22] destabilization of this region is likely to be responsible for accelerating the misfolding of the protein. Importantly, several other pathogenic mutations that destabilize moPrP all result in one common structural perturbation: they cause increased structural dynamics in α1 and the loop between α1 and β2.[22] Moreover, these pathogenic mutations result in an increase in the rate of misfolding to oligomer, in a manner that correlates very well with the increased structural dynamics in α1 and the loop between α1 and β2. Hence, the increased rate of misfolding to oligomers of T182A moPrP could be due to increased structural dynamics in α1 and the loop between α1 and β2, as well as to the destabilization of the α2−α3 region.

The most stable part of the core in native monomeric wt moPrP is known to be the α3 region, and the same region becomes even more stable upon misfolding to oligomer, presumably because it undergoes conformational conversion to β-structure.[22] This region was seen to be significantly less stable in monomeric T182A moPrP (Figures 5 and 6). It is likely that the decrease in the stability of α3 in T182A moPrP is coupled to the exposure of the hydrophobic core of the protein and facilitates its conformational conversion to β-structure. This could be the reason why the misfolding rate of T182A is so significantly faster than that of the wt protein and is faster than that predicted by the destabilization of only α1 and the loop between α1 and β2.[22]

For many proteins, it has been shown that the free energy of opening of the most stable core structure to HDX matches the free energy of global unfolding determined from denaturant-induced equilibrium unfolding experiments.[54] The free energy of opening of structure to HDX is given by $RT \ln P_f$. The average value for P_f for the most stable core region (α3) of T182A moPrP is 28 (Table 2). The free energy of opening of α3 to HDX in T182A moPrP is therefore 2 kcal mol^{-1}, which is similar to the value of the free energy of global unfolding determined from the urea-induced equilibrium experiment (Table 1). In the case of wt moPrP, the value of P_f for α3 was too high to be determined for the most stable sequence segment. However, in an earlier more comprehensive measurement of HDX at pH 4, it was shown that the free energy of opening of α3 to HDX matched the free energy of global unfolding for wt moPrP, too.[54]

Subdomain separation, of β1−α1−β2 from α2−α3, has been shown to be a prerequisite for oligomerization: locking these two subdomains by disulfide linkage prevents ovine PrP oligomerization.[67] Subdomain separation would lead to the disruption of interactions between the two subdomains and, hence, their increased level of destabilization. Chemical chaperones or drug molecules, which are known to bind to both α1 and parts of the α2−α3 region,[68,69] have therapeutic potencies for PrP presumably because they lock the PrP structure and prevent its subdomain separation.

Role of MG-like Forms in Misfolding of PrP to Oligomers. In the study presented here, it has been shown that T182A moPrP exists as a MG-like form with drastically reduced global stability as well as cooperativity of unfolding, and with increased structural dynamics. MG forms of proteins in which solvent does not penetrate the hydrophobic core appear to have protection against HDX like those of native forms.[70] On the other hand, MG forms that have their core accessible to solvent have protection against HDX substantially lower than that of native forms.[71−73] T182A moPrP has drastically reduced protection against HDX in comparison to that of wt moPrP. This suggests that the core of T182A moPrP is accessible to solvent. This observation is supported by ANS binding studies. ANS binds to T182A moPrP, but not to wt moPrP, indicating that T182A moPrP has solvent accessible hydrophobic surfaces. Moreover, T182A moPrP shows a drastic reduction in *m*-values. MG forms are known to have low *m*-values compared to those of native proteins.[42,55] Methionine oxidation of PrP is also known to disrupt its structural core, leading to the formation of a MG form, which is competent to form misfolded oligomers.[39] The MG form formed upon methionine oxidation is structurally similar to the acid-induced MG form.[39] Interestingly, the acid-induced MG form of PrP,[40] which is a native-like intermediate and has been shown to be a direct precursor to misfolded oligomers,[40,41] appears to be structurally similar to T182A moPrP. These studies thus indicate that the formation of a MG form might be an early step on the pathway of misfolding of PrP to oligomers.

AUTHOR INFORMATION

Corresponding Author

*National Centre for Biological Sciences, Tata Institute of Fundamental Research, Bengaluru 560065, India. E-mail: jayant@ncbs.res.in. Fax: 91-80-23636662.

Funding

This work was funded by the Tata Institute of Fundamental Research and by the Department of Biotechnology, Government of India. J.B.U. is a recipient of a J. C. Bose National Fellowship from the Government of India.

Notes

The authors declare no competing financial interest.

ACKNOWLEDGMENTS

The AFM images were collected at the Central Imaging Facility of the National Centre for Biological Sciences.

ABBREVIATIONS

PrP^C, cellular prion protein; PrP^{Sc}, scrapie PrP; PrP, recombinant prion protein; moPrP, mouse prion protein; *Prnp*, prion protein gene; fCJD, familial Creutzfeldt-Jakob disease; wt, wild-type; HDX, hydrogen−deuterium exchange; MS, mass spectrometry; α1, helix 1; α2, helix 2; α3, helix 3; β1, β-strand 1; β2, β-strand 2; SEC, size exclusion chromatography; CD, circular dichroism; DLS, dynamic light scattering; ANS, 8-anilinonaphthalene-1-sulfonic acid; MG, molten globule.

REFERENCES

(1) Prusiner, S. B. (1991) Molecular biology of prion diseases. *Science 252*, 1515−1522.

(2) Stimson, E., Hope, J., Chong, A., and Burlingame, A. L. (1999) Site-specific characterization of the N-linked glycans of murine prion protein by high-performance liquid chromatography/electrospray mass

DOI: 10.1021/acs.biochem.5b01266
Biochemistry 2016, 55, 459−469

spectrometry and exoglycosidase digestions. *Biochemistry 38*, 4885−4895.
(3) Prusiner, S. B. (1998) Prions. *Proc. Natl. Acad. Sci. U. S. A. 95*, 13363−13383.
(4) Aguzzi, A., and Polymenidou, M. (2004) Mammalian prion biology: One century of evolving concepts. *Cell 116*, 313−327.
(5) Baskakov, I. V., Legname, G., Baldwin, M. A., Prusiner, S. B., and Cohen, F. E. (2002) Pathway complexity of prion protein assembly into amyloid. *J. Biol. Chem. 277*, 21140−21148.
(6) Jain, S., and Udgaonkar, J. B. (2008) Evidence for stepwise formation of amyloid fibrils by the mouse prion protein. *J. Mol. Biol. 382*, 1228−1241.
(7) Jain, S., and Udgaonkar, J. B. (2011) Prion protein aggregation. *Curr. Sci. 101*, 1311−1327.
(8) Mallucci, G., Dickinson, A., Linehan, J., Klöhn, P. C., Brandner, S., and Collinge, J. (2003) Depleting neuronal PrP in prion infection prevents disease and reverses spongiosis. *Science 302*, 871−874.
(9) Novitskaya, V., Bocharova, O. V., Bronstein, I., and Baskakov, I. V. (2006) Amyloid fibrils of mammalian prion protein are highly toxic to cultured cells and primary neurons. *J. Biol. Chem. 281*, 13828−13836.
(10) Piccardo, P., Manson, J. C., King, D., Ghetti, B., and Barron, R. M. (2007) Accumulation of prion protein in the brain that is not associated with transmissible disease. *Proc. Natl. Acad. Sci. U. S. A. 104*, 4712−4717.
(11) Kristiansen, M., Deriziotis, P., Dimcheff, D. E., Jackson, G. S., Ovaa, H., Naumann, H., Clarke, A. R., van Leeuwen, F. W., Menéndez-Benito, V., Dantuma, N. P., Portis, J. L., Collinge, J., and Tabrizi, S. J. (2007) Disease-associated prion protein oligomers inhibit the 26S proteasome. *Mol. Cell 26*, 175−188.
(12) Simoneau, S., Rezaei, H., Sales, N., Kaiser-Schulz, G., Lefebvre-Roque, M., Vidal, C., Fournier, J. G., Comte, J., Wopfner, F., Grosclaude, J., Schätzl, H., and Lasmézas, C. I. (2007) In vitro and in vivo neurotoxicity of prion protein oligomers. *PLoS Pathog. 3*, e125.
(13) Tixador, P., Herzog, L., Reine, F., Jaumain, E., Chapuis, J., Le Dur, A., Laude, H., and Béringue, V. (2010) The physical relationship between infectivity and prion protein aggregates is strain-dependent. *PLoS Pathog. 6*, e1000859.
(14) Anaya, Z. E., Savistchenko, J., Massonneau, V., Lacroux, C., Andreoletti, O., and Vilette, D. (2011) Recovery of small infectious PrP^{res} aggregates from prion-infected cultured cells. *J. Biol. Chem. 286*, 8141−8148.
(15) Choi, Y. P., Gröner, A., Ironside, J. W., and Head, M. W. (2011) Correlation of Polydispersed Prion Protein and Characteristic Pathology in the Thalamus in Variant Creutzfeldt-Jakob Disease: Implication of Small Oligomeric Species. *Brain Pathol. 21*, 298−307.
(16) Sajnani, G., Silva, C. J., Ramos, A., Pastrana, M. A., Onisko, B. C., Erickson, M. L., Antaki, E. M., Dynin, I., Vázquez-Fernández, E., Sigurdson, C. J., Carter, J. M., and Requena, J. R. (2012) PK-sensitive PrP^{Sc} is infectious and shares basic structural features with PK-resistant PrP^{Sc}. *PLoS Pathog. 8*, e1002547.
(17) Laferrière, F., Tixador, P., Moudjou, M., Chapuis, J., Sibille, P., Herzog, L., Reine, F., Jaumain, E., Laude, H., Rezaei, H., and Béringue, V. (2013) Quaternary structure of pathological prion protein as a determining factor of strain-specific prion replication dynamics. *PLoS Pathog. 9*, e1003702.
(18) Sandberg, M. K., Al-Doujaily, H., Sharps, B., De Oliveira, M. W., Schmidt, C., Richard-Londt, A., Lyall, S., Linehan, J. M., Brandner, S., Wadsworth, J. D., Clarke, A. R., and Collinge, J. (2014) Prion neuropathology follows the accumulation of alternate prion protein isoforms after infective titre has peaked. *Nat. Commun. 5*, 4347.
(19) Singh, J., Sabareesan, A. T., Mathew, M. K., and Udgaonkar, J. B. (2012) Development of the structural core and of conformational heterogeneity during the conversion of oligomers of the mouse prion protein to worm like amyloid fibrils. *J. Mol. Biol. 423*, 217−231.
(20) Miller, M. B., Wang, D. W., Wang, F., Noble, G. P., Ma, J., Woods, V. L., Li, S., and Supattapone, S. (2013) Cofactor molecules induce structural transformation during infectious prion formation. *Structure 21*, 2061−2068.
(21) Singh, J., and Udgaonkar, J. B. (2015) Molecular Mechanism of the Misfolding and Oligomerization of the Prion Protein: Current Understanding and Its Implications. *Biochemistry 54*, 4431−4442.
(22) Singh, J., and Udgaonkar, J. B. (2015) Structural Effects of Multiple Pathogenic Mutations Suggest a Model for the Initiation of Misfolding of the Prion Protein. *Angew. Chem., Int. Ed. 54*, 7529−7533.
(23) Singh, J., Kumar, H., Sabareesan, A. T., and Udgaonkar, J. B. (2014) Rational stabilization of helix 2 of the prion protein prevents its misfolding and oligomerization. *J. Am. Chem. Soc. 136*, 16704−16707.
(24) Bjorndahl, T. C., Zhou, G. P., Liu, X., Perez-Pineiro, R., Semenchenko, V., Saleem, F., Acharya, S., Bujold, A., Sobsey, C. A., and Wishart, D. S. (2011) Detailed Biophysical Characterization of the Acid-Induced PrPc to PrPβ Conversion Process. *Biochemistry 50*, 1162−1173.
(25) Singh, J., and Udgaonkar, J. B. (2013) Dissection of conformational conversion events during prion amyloid fibril formation using hydrogen exchange and mass spectrometry. *J. Mol. Biol. 425*, 3510−3521.
(26) Nitrini, R., Rosemberg, S., Passos-Bueno, M. R., Teixeira da Silva, L. S., Iughetti, P., Papadopoulos, M., Carrilho, P. M., Caramelli, P., Albrecht, S., Zatz, M., and LeBlanc, A. (1997) Familial spongiform encephalopathy associated with a novel prion protein gene mutation. *Ann. Neurol. 42*, 138−146.
(27) Grasbon-Frodl, E., Lorenz, H., Mann, U., Nitsch, R. M., Windl, O., and Kretzschmar, H. A. (2004) Loss of glycosylation associated with the T183A mutation in human prion disease. *Acta Neuropathol. 108*, 476−484.
(28) Zou, R. S., Fujioka, H., Guo, J. P., Xiao, X., Shimoji, M., Kong, C., Chen, C., Tasnadi, M., Voma, C., Yuan, J., Moudjou, M., Laude, H., Petersen, R. B., and Zou, W. Q. (2011) Characterization of spontaneously generated prion-like conformers in cultured cells. *Aging 3*, 968−984.
(29) Jackson, W. S., Borkowski, A. W., Faas, H., Steele, A. D., King, O. D., Watson, N., Jasanoff, A., and Lindquist, S. (2009) Spontaneous generation of prion infectivity in fatal familial insomnia knockin mice. *Neuron 63*, 438−450.
(30) Khurana, R., and Udgaonkar, J. B. (1994) Equilibrium unfolding studies of barstar: evidence for an alternative conformation which resembles a molten globule. *Biochemistry 33*, 106−115.
(31) Nath, U., and Udgaonkar, J. B. (1995) Perturbation of a tertiary hydrogen bond in barstar by mutagenesis of the sole His residue to Gln leads to accumulation of at least one equilibrium folding intermediate. *Biochemistry 34*, 1702−1713.
(32) Sauder, J. M., MacKenzie, N. E., and Roder, H. (1996) Kinetic mechanism of folding and unfolding of Rhodobacter capsulatus cytochrome c_2. *Biochemistry 35*, 16852−16862.
(33) Booth, D. R., Sunde, M., Bellotti, V., Robinson, C. V., Hutchinson, W. L., Fraser, P. E., Hawkins, P. N., Dobson, C. M., Radford, S. E., Blake, C. C., and Pepys, M. B. (1997) Instability, unfolding and aggregation of human lysozyme variants underlying amyloid fibrillogenesis. *Nature 385*, 787−793.
(34) Hamid Wani, A. H., and Udgaonkar, J. B. (2006) HX-ESI-MS and Optical Studies of the Unfolding of Thioredoxin Indicate Stabilization of a Partially Unfolded, Aggregation-Competent Intermediate at Low pH. *Biochemistry 45*, 11226−11238.
(35) Canet, D., Last, A. M., Tito, P., Sunde, M., Spencer, A., Archer, D. B., Redfield, C., Robinson, C. V., and Dobson, C. M. (2002) Local cooperativity in the unfolding of an amyloidogenic variant of human lysozyme. *Nat. Struct. Biol. 9*, 308−315.
(36) Juneja, J., Bhavesh, N. S., Udgaonkar, J. B., and Hosur, R. V. (2002) NMR Identification and Characterization of the Flexible Regions in the 160 kD Molten Globule-Like Aggregate of Barstar at Low pH. *Biochemistry 41*, 9885−9899.
(37) Carrotta, R., Bauer, R., Waninge, R., and Rischel, C. (2001) Conformational characterization of oligomeric intermediates and aggregates in β-lactoglobulin heat aggregation. *Protein Sci. 10*, 1312−1318.
(38) Uversky, V. N., Lee, H. J., Li, J., Fink, A. L., and Lee, S. J. (2001) Stabilization of partially folded conformation during α-synuclein

DOI: 10.1021/acs.biochem.5b01266
Biochemistry 2016, 55, 459−469

oligomerization in both purified and cytosolic preparations. *J. Biol. Chem. 276*, 43495−43498.
(39) Younan, N. D., Nadal, R. C., Davies, P., Brown, D. R., and Viles, J. H. (2012) Methionine oxidation perturbs the structural core of the prion protein and suggests a generic misfolding pathway. *J. Biol. Chem. 287*, 28263−28275.
(40) Honda, R. P., Yamaguchi, K. I., and Kuwata, K. (2014) Acid-induced Molten Globule State of a Prion Protein: Crucial role of strand 1-helix 1-strand 2 segment. *J. Biol. Chem. 289*, 30355−30363.
(41) Honda, R. P., Xu, M., Yamaguchi, K. I., Roder, H., and Kuwata, K. (2015) A Native-like Intermediate Serves as a Branching Point between the Folding and Aggregation Pathways of the Mouse Prion Protein. *Structure 23*, 1735−1742.
(42) Kuwajima, K. (1989) The molten globule state as a clue for understanding the folding and cooperativity of globular-protein structure. *Proteins: Struct., Funct., Genet. 6*, 87−103.
(43) Liemann, S., and Glockshuber, R. (1999) Influence of amino acid substitutions related to inherited human prion diseases on the thermodynamic stability of the cellular prion protein. *Biochemistry 38*, 3258−3267.
(44) Madampage, C. A., Määttänen, P., Marciniuk, K., Brownlie, R., Andrievskaia, O., Potter, A., Cashman, N. R., Lee, J. S., and Napper, S. (2013) Binding of bovine T194A PrP(C) by PrP(Sc)-specific antibodies: potential implications for immunotherapy of familial prion diseases. *Prion 7*, 301−311.
(45) Chebaro, Y., and Derreumaux, P. (2009) The conversion of helix H2 to beta-sheet is accelerated in the monomer and dimer of the prion protein upon T183A mutation. *J. Phys. Chem. B 113*, 6942−6948.
(46) van der Kamp, M. W., and Daggett, V. (2010) Pathogenic mutations in the hydrophobic core of the human prion protein can promote structural instability and misfolding. *J. Mol. Biol. 404*, 732−748.
(47) Hong, D., Xiong, W., Chang, J., and Jiang, C. (2011) The role of the C-terminus of human a-synuclein: Intra-disulfide bonds between the C-terminus and other regions stabilize non-fibrillar monomeric isomers. *FEBS Lett. 585*, 561−566.
(48) Sabareesan, A. T., and Udgaonkar, J. B. (2014) Amyloid Fibril Formation by the Chain B Subunit of Monellin Occurs by a Nucleation-Dependent Polymerization Mechanism. *Biochemistry 53*, 1206−1217.
(49) Morillas, M., Vanik, D. L., and Surewicz, W. K. (2001) On the mechanism of α-helix to β-sheet transition in the recombinant prion protein. *Biochemistry 40*, 6982−6987.
(50) Moulick, R., and Udgaonkar, J. B. (2014) Thermodynamic Characterization of the Unfolding of the Prion Protein. *Biophys. J. 106*, 410−420.
(51) Bai, Y., Milne, J. S., Mayne, L., and Englander, S. W. (1993) Primary structure effects on peptide group hydrogen exchange. *Proteins: Struct., Funct., Genet. 17*, 75−86.
(52) Chetty, P. S., Mayne, L., Lund-Katz, S., Stranz, D., Englander, S. W., and Phillips, M. C. (2009) Helical structure and stability in human apolipoprotein A-I by hydrogen exchange and mass spectrometry. *Proc. Natl. Acad. Sci. U. S. A. 106*, 19005−19010.
(53) Semisotnov, G. V., Rodionova, N., Razgulyaev, O. I., Uversky, V. N., Gripas', A. F., and Gilmanshin, R. I. (1991) Study of the "molten globule" intermediate state in protein folding by a hydrophobic fluorescent probe. *Biopolymers 31*, 119−128.
(54) Moulick, R., Das, R., and Udgaonkar, J. B. (2015) Partially unfolded forms of the prion protein populated under misfolding-promoting conditions: characterization by hydrogen exchange mass spectrometry and NMR. *J. Biol. Chem. 290*, 25227−25240.
(55) Hoofnagle, A. N., Resing, K. A., and Ahn, N. G. (2003) Protein analysis by hydrogen exchange mass spectrometry. *Annu. Rev. Biophys. Biomol. Struct. 32*, 1−25.
(56) Nishii, I., Kataoka, M., and Goto, Y. (1995) Thermodynamic stability of the molten globule states of apomyoglobin. *J. Mol. Biol. 250*, 223−238.
(57) Maiti, N. R., and Surewicz, W. K. (2001) The role of disulfide bridge in the folding and stability of the recombinant human prion protein. *J. Biol. Chem. 276*, 2427−2431.
(58) Swietnicki, W., Morillas, M., Chen, S. G., Gambetti, P., and Surewicz, W. K. (2000) Aggregation and Fibrillization of the Recombinant Human Prion Protein huPrP90−231. *Biochemistry 39*, 424−431.
(59) Jain, S., and Udgaonkar, J. B. (2010) Salt-induced modulation of the pathway of amyloid fibril formation by the mouse prion protein. *Biochemistry 49*, 7615−7624.
(60) Apetri, A. C., Vanik, D. L., and Surewicz, W. K. (2005) Polymorphism at residue 129 modulates the conformational conversion of the D178N variant of human prion protein 90−231. *Biochemistry 44*, 15880−15888.
(61) Breydo, L., Bocharova, O. V., Makarava, N., Salnikov, V. V., Anderson, M., and Baskakov, I. V. (2005) Methionine Oxidation Interferes with Conversion of the Prion Protein into the Fibrillar Proteinase K-Resistant Conformation. *Biochemistry 44*, 15534−15543.
(62) Dutta, A., Chen, S., and Surewicz, W. K. (2013) The effect of β2-α2 loop mutation on amyloidogenic properties of the prion protein. *FEBS Lett. 587*, 2918−2923.
(63) Lim, W. A., and Sauer, R. T. (1989) Alternative packing arrangements in the hydrophobic core of λrepresser. *Nature 339*, 31−36.
(64) Lim, W. A., and Sauer, R. T. (1991) The role of internal packing interactions in determining the structure and stability of a protein. *J. Mol. Biol. 219*, 359−376.
(65) Ratnaparkhi, G. S., and Varadarajan, R. (2000) Thermodynamic and Structural Studies of Cavity Formation in Proteins Suggest That Loss of Packing Interactions Rather Than the Hydrophobic Effect Dominates the Observed Energetics. *Biochemistry 39*, 12365−12374.
(66) Kong, Q., Mills, J. L., Kundu, B., Li, X., Qing, L., Surewicz, K., Cali, I., Huang, S., Zheng, M., Swietnicki, W., Sönnichsen, F. D., Gambetti, P., and Surewicz, W. K. (2013) Thermodynamic stabilization of the folded domain of prion protein inhibits prion infection in vivo. *Cell Rep. 4*, 248−254.
(67) Eghiaian, F., Daubenfeld, T., Quenet, Y., van Audenhaege, M., Bouin, A. P., van der Rest, G., Grosclaude, J., and Rezaei, H. (2007) Diversity in prion protein oligomerization pathways results from domain expansion as revealed by hydrogen/deuterium exchange and disulfide linkage. *Proc. Natl. Acad. Sci. U. S. A. 104*, 7414−7419.
(68) Antonyuk, S. V., Trevitt, C. R., Strange, R. W., Jackson, G. S., Sangar, D., Batchelor, M., Cooper, S., Fraser, C., Jones, S., Georgiou, T., Khalili-Shirazi, A., Clarke, A. R., Hasnain, S. S., and Collinge, J. (2009) Crystal structure of human prion protein bound to a therapeutic antibody. *Proc. Natl. Acad. Sci. U. S. A. 106*, 2554−2258.
(69) Xu, Z., Adrover, M., Pastore, A., Prigent, S., Mouthon, F., Comoy, E., Rezaei, H., and Deslys, J. P. (2011) Mechanistic insights into cellular alteration of prion by poly-d-lysine: the role of H2H3 domain. *FASEB J. 25*, 3426−3435.
(70) Kjellsson, A., Sethson, I., and Jonsson, B. H. (2003) Hydrogen exchange in a large 29 kD protein and characterization of molten globule aggregation by NMR. *Biochemistry 42*, 363−374.
(71) Hughson, F. M., Wright, P. E., and Baldwin, R. L. (1990) Structural characterization of a partly folded apomyoglobin intermediate. *Science 249*, 1544−1548.
(72) Morozova, L. A., Haynie, D. T., Arico-Muendel, C., Van Dael, H., and Dobson, C. M. (1995) Structural basis of the stability of a lysozyme molten globule. *Nat. Struct. Biol. 2*, 871−875.
(73) Kobashigawa, Y., Demura, M., Koshiba, T., Kumaki, Y., Kuwajima, K., and Nitta, K. (2000) Hydrogen exchange study of canine milk lysozyme: Stabilization mechanism of the molten globule. *Proteins: Struct., Funct., Genet. 40*, 579−589.
(74) Gossert, A. D., Bonjour, S., Lysek, D. A., Fiorito, F., and Wüthrich, K. (2005) Prion protein NMR structures of elk and of mouse/elk hybrids. *Proc. Natl. Acad. Sci. U. S. A. 102*, 646−650.

DOI: 10.1021/acs.biochem.5b01266
Biochemistry 2016, 55, 459−469